Supporting Information for Publication

Supplementary Figures and tables

Supplementary table 1

X-ray source	LMB Bruker	
Wavelength λ (Å)	1.54179	
Space group	$P2_1$	
Unit cell (a Å, b Å, c Å)	60.75 73.95 170.50 90.0 91.46 90.0	
Resolution shell (Å)	50-2.07	
Measurements	3335855	
Average I/σI	8.26	0.75
Unique reflections	140066	9539
Completeness (%)	76.8	52.3
R_{merge} (%)[§]	10.6	70.1
R_{cryst} (%)*	25.0	
R_{free} (%)[†]	26.8	
RMS deviation[¶]	0.019Å (1.88˚)	
B factors[‡] (Å^2)	37.35, 38.43, 32.92, 36.33	
Residues	1540	
Water molecules	295	
PDB code	2vzk	

[§] $R_{merge} = \sum_j\sum_h| I_{h,j}-\langle I_h\rangle| / \sum_j\sum_h\langle I_h\rangle \times 100$

* $R_{cryst} = \sum|\,|F_{obs}| - |F_{calc}|\,| / \sum|F_{obs}| \times 100$

[†] R_{free} = based on 5% of the total reflections.

[¶] RMS deviation from ideality for bonds (followed by the value for angles).

[‡] Average *B* factors in order: main chain, side chain, substrate and solvent.

Supplementary Figure 1

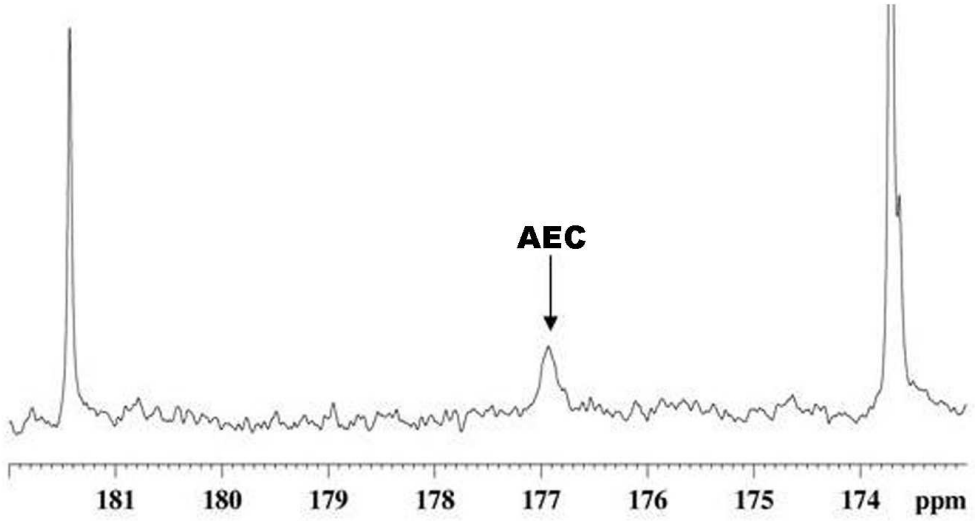

Supplementary Figure 2

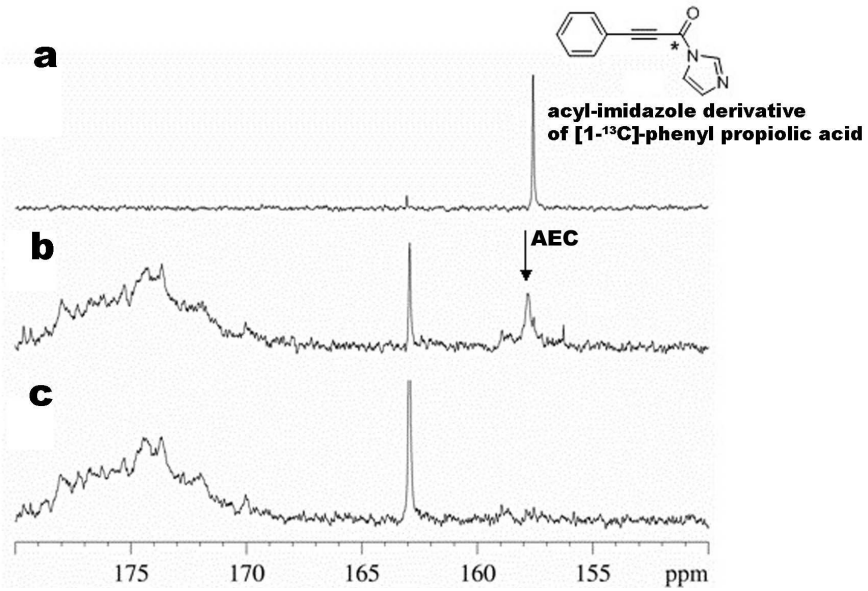

Supplementary Figure 3

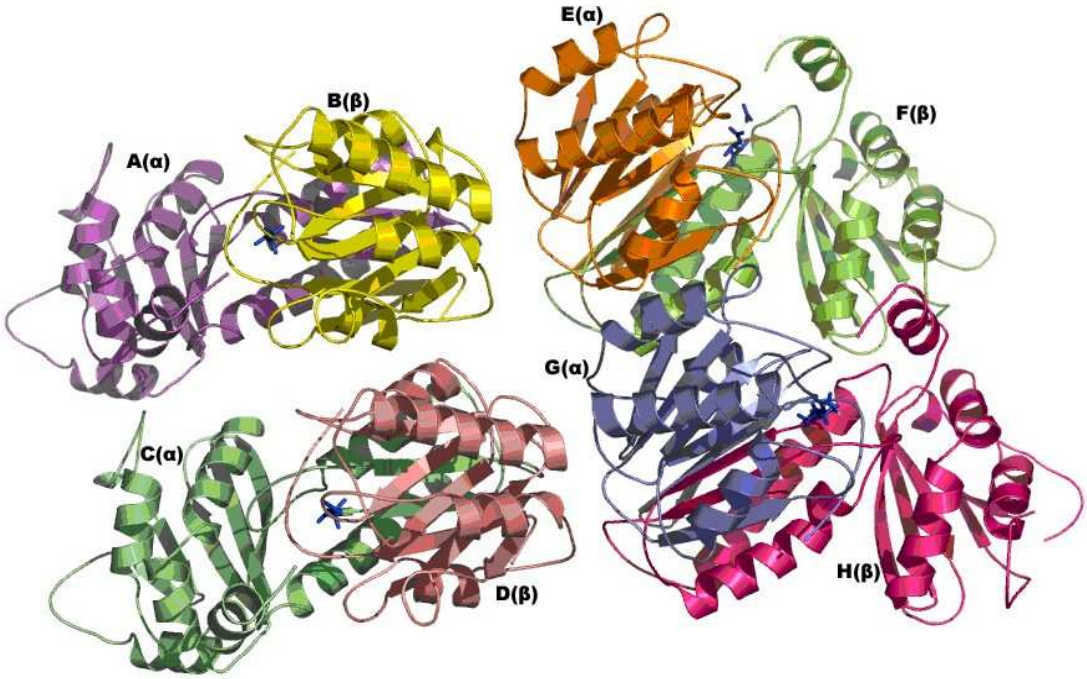

Supplementary Figure 4

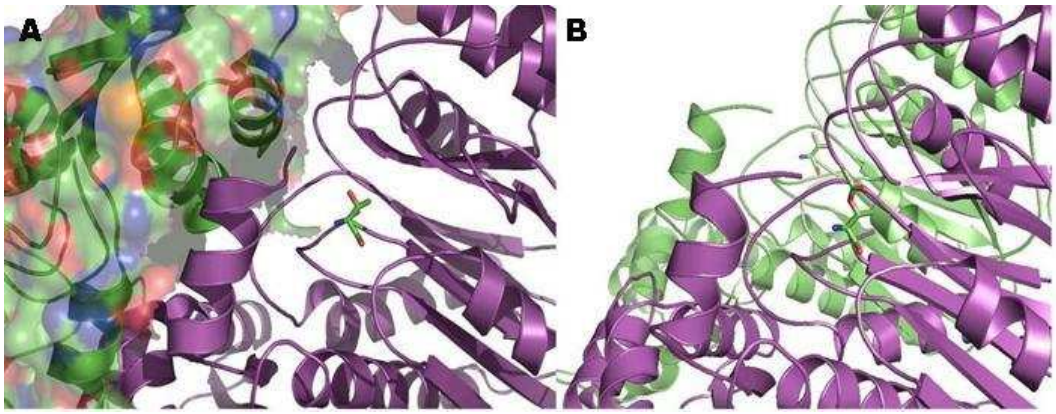

Supplementary Figure 5

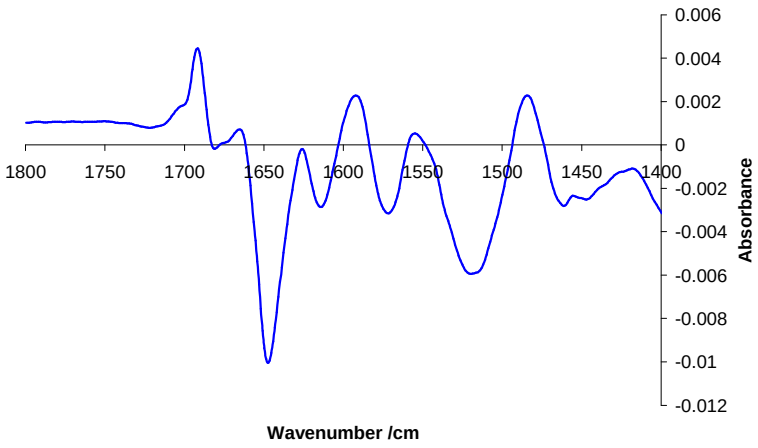

Supplementary Figure 6

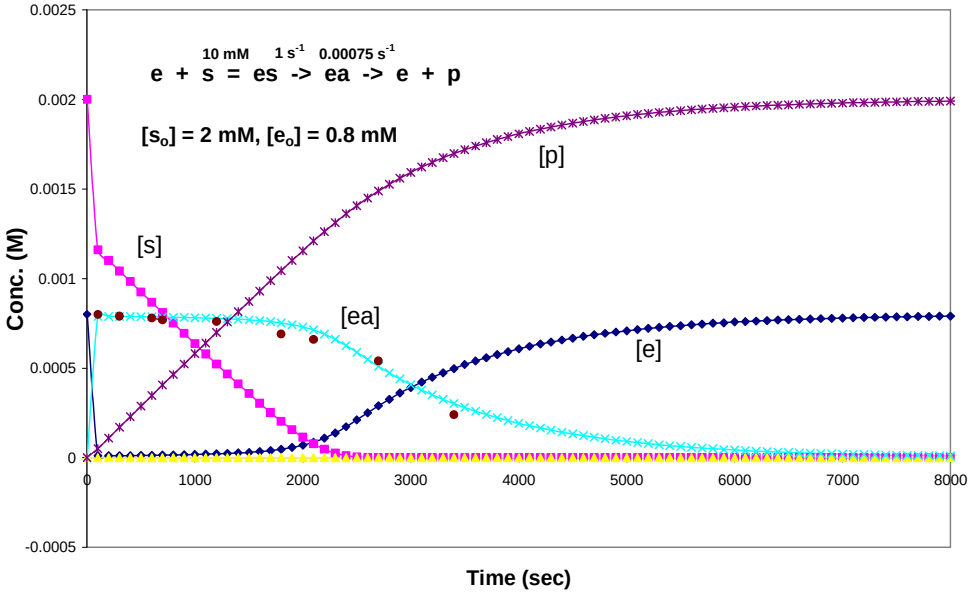

Supplementary Figure 7:

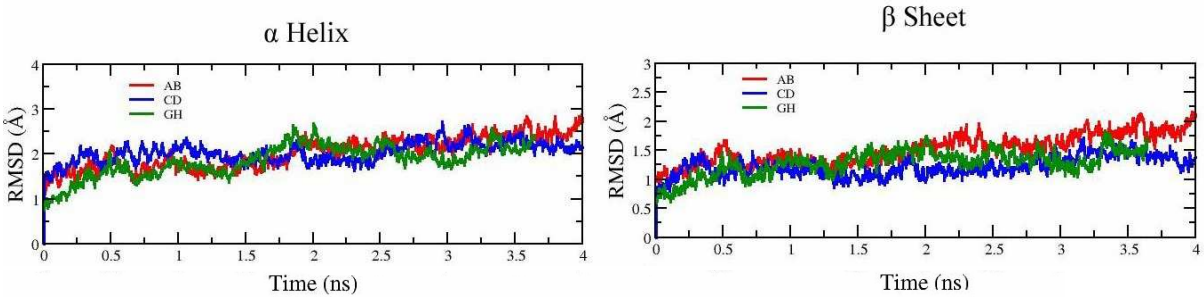

Supplementary figures and table legends:

Supp Table 1: Data collection and statistics for the crystal structure of acyl-OAT2.

Supp Figure 1: ^{13}C NMR spectra showing the assigned acyl-enzyme complex at 176.9 ppm (indicated by an arrow). The other resonances in the spectrum correspond to the substrate ^{13}C- acyl-*N*-α-acetyl-L-glutamate resonance at 174.6 ppm, and product ^{13}C acetate resonance at 181.4 ppm.

Supp Figure 2: NMR experiments with chymotrypsin. (a) Spectrum for the imidazole derivative of ^{13}C-phenyl propiolic acid. (b) The reaction of chymotrypsin with ^{13}C-phenyl propiolic acid at t = 0, and (c) after incubation of the reaction mixture for 10 min. The arrow indicates the resonance corresponding to the assigned chymotrypsin acyl-enzyme complex. The broad resonance between 170-180 ppm in (b) and (c) corresponds to protein background.

Supp Figure 3: View from the acyl-OAT2 crystal structure showing the four subunits/eight chains of OAT2 acyl-enzyme complex. The AB, CD, EF and GH molecules are shown in different colours corresponding to the eight different chains. Thr-181 is in blue sticks.

Supp Figure 4: Comparison of the unmodified OAT2 and acyl-OAT2 crystal structures showing the active site regions. (a) The entrance of the OAT2 active site is blocked by the *C*-terminal domain of a neighbouring molecule (shown in a surface view) in the unmodified OAT2 structure. (b) In the acyl-OAT2 structure the entrance to the active site is open to solvent. Thr-181 is in blue sticks.

Supp Figure 5: Difference (^{12}C=O minus ^{13}C=O) IR spectra of the OAT2 acyl-enzyme complex produced by reaction with *N*-α-acetyl-L-glutamate. The broad absorption band at 1690-1710cm^{-1} is assigned as the acyl-enzyme complex of OAT2.

Supp Figure 6: Kinetic analysis of the OAT2 reaction with *N*-α-acetyl-L-glutamate as measured by IR, indicating the steady state nature of the acyl-enzyme complex (upto 1700 sec). The plot was generated by GEPASI {Mendes, 1997 #527}. Experimental values of initial substrate [S] and enzyme [e] concentration along with the acyl-enzyme degradation time course [ea] were inputted into GEPASI which generated the curves for product formation [p] and enzyme regeneration [e]. The inset shows the mechanistic model employed.

Supp Figure 7: R.m.s.d values for α-helix and β-sheet regions of acyl-OAT2 compared to the crystallographic coordinates for the three molecules, AB, CD and GH over an molecular dynamics simulation of 4 ns.